Shapes of flux domains in the intermediate state of type-I superconductors

Alan T. Dorsey*
Department of Physics, University of Florida, Gainesville, Florida 32611

Raymond E. Goldstein†
Department of Physics and Program in Applied Mathematics, University of Arizona, Tucson, Arizona 85721

(Received 17 April 1997; revised manuscript received 3 September 1997)

In the intermediate state of a thin type-I superconductor magnetic flux penetrates in a disordered set of highly branched and fingered macroscopic domains. To understand these shapes, we study in detail a recently proposed ''current-loop'' model [R. E. Goldstein, D. P. Jackson, and A. T. Dorsey, Phys. Rev. Lett. **76**, 3818 (1996)] that models the intermediate state as a collection of tense current ribbons flowing along the superconducting-normal interfaces and subject to the constraint of global flux conservation. The validity of this model is tested through a detailed reanalysis of Landau's original conformal mapping treatment of the laminar state, in which the superconductor-normal interfaces are flared within the slab, and of a closely related straight-lamina model. A simplified dynamical model is described that elucidates the nature of possible shape instabilities of flux stripes and stripe arrays, and numerical studies of the highly nonlinear regime of those instabilities demonstrate patterns like those seen experimentally. Of particular interest is the buckling instability commonly seen in the intermediate state. The free-boundary approach further allows for a calculation of the elastic properties of the laminar state, which closely resembles that of smectic liquid crystals. We suggest several experiments to explore flux domain shape instabilities, including an Eckhaus instability induced by changing the out-of-plane magnetic field and an analog of the Helfrich-Hurault instability of smectics induced by an in-plane field. [S0163-1829(98)01005-4]

I. INTRODUCTION

A long-standing problem in macroscopic superconductivity is that of understanding the complex patterns of flux penetration in the intermediate state of a type-I superconductor. This state occurs when a thin superconducting slab is placed in a perpendicular magnetic field. Unlike type-II superconductors, in which the field penetrates through tubes each with a quantum of magnetic flux, type-I systems form intricately branched and fingered *macroscopic* flux domains.[1–3] Thus, instead of a Meissner phase, in which the magnetic induction $\mathbf{B}=\mathbf{0}$ uniformly, the demagnetizing effects of the large aspect ratio force the sample to break up into regions, some of which are uniformly superconducting (with $\mathbf{B}=\mathbf{0}$ inside) and others that are normal ($\mathbf{B}\neq\mathbf{0}$). Figure 1 shows a typical example of these patterns observed by decoration.[3] Other imaging techniques (Hall probes[4] and magneto-optics[5]) reveal similar structures.

The sample in Fig. 1 has an applied field H_a close to the critical field H_c at which the sample would be completely normal, so the minority phase is superconducting. Similar patterns are observed when H_a/H_c is very small, but the minority phase is normal; the sample consists of branched *flux domains* in a matrix of superconductor. These have a characteristic field-dependent finger width and threefold vertices. More ordered domains may be observed in the presence of a small in-plane component of the applied field.[6]

The domain morphology depends on the path in field-temperature space through which the sample has been brought to a given point.[3] For instance, cooling in zero field below the transition temperature and then applying the field tends to produce patterns in which normal domains are embedded in a matrix of superconductor, whereas when the same point in T-H space is reached by cooling below T_c in a fixed field the normal domains connect to the sample edges.[1] These observations suggest that the patterns are not true ground states of the system: The sample is not in true thermodynamic equilibrium.

Despite their ubiquity, until recently there has been no theoretical explanation for these patterns. The earliest attempt, prior to the experiments described above, was Landau's treatment of the laminar state,[7] a periodic array of superconducting and normal domains (Fig. 2). Exploiting the translational invariance of the pattern along the stripes, the cross-sectional shape of the domain walls and the bending of the magnetic field lines become purely two-dimensional problems solved by conformal mapping techniques, yielding the free energy as a function of lamina spacing, applied field,

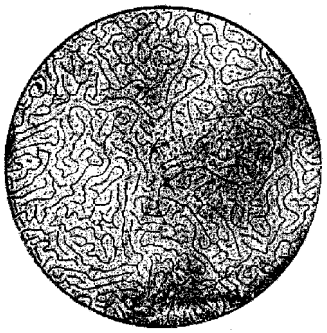

FIG. 1. Intermediate state of indium, in which superconducting regions (black) are decorated with niobium. The applied field is close to the critical field ($H_a/H_c=0.931$). Adapted from Haenssler and Rinderer (Ref. 3).

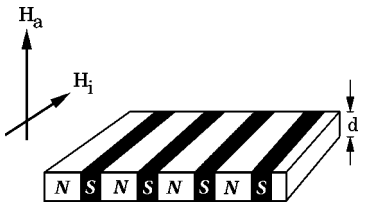

FIG. 2. Laminar state in a thin slab. The applied field H_a is normal to the slab. An ordered laminar structure is obtained with an additional in-plane component H_i.

superconductor-normal surface energy, and slab thickness.

This free energy depends on two parameters: the area fraction of the normal state and the repeat distance of the structure. For thick slabs, one finds that the equilibrium area fraction is set by the reduced field $h=H_a/H_c$. Deep within the slab the domain walls are aligned with the field, but they flare along with the magnetic field lines near the surface. Subsequent experiments[1–3] found field-dependent widths in good agreement with theory. Stability calculations about this state are, however, precluded by the reliance on conformal mapping techniques; no calculations of this type have been performed. Subsequently, and in light of experiments showing nearly circular flux domains, several calculations of the energies of periodic arrays of simple geometric structures were performed,[8] showing that there is little thermodynamic driving force preferring one over the other. None of these theories offers an explanation for the appearance of branched flux domains.

The features of disordered domain shapes and path dependence to the patterns show that an understanding of the intermediate state requires a theory that treats the superconductor-normal (SN) interfaces as a *free-boundary* problem and addresses the *dynamics* of those interfaces. The relevance of an interfacial representation, rather than a more microscopic approach based on dynamics of the superconducting order parameter and vector potential, is clear by the strong *separation of scales* between the domain size (typically fractions of a millimeter) and the width of the SN interface. For a strongly type-I superconductor the width is set by the coherence length ξ, which is on the order of 0.2 μm.

Recent studies[9,10] have emphasized strong connections between the motion of SN interfaces in a magnetic field and the dynamics of solid-liquid interfaces during solidification. The key to this relationship is the diffusion of magnetic field in the normal state,[11] analogous to the diffusion of latent heat in crystallization. This suggests that a *diffusional instability* such as the Mullins-Sekerka instability[12] should occur during flux invasion. Numerical studies of the time-dependent Ginzburg-Landau model confirmed these instabilities, which can lead to highly ramified domain patterns.

Asymptotic methods[13] also show that in the sharp-interface limit it is possible to integrate out the magnetic field contributions and arrive at a nonlocal free-boundary theory for the SN interface alone. The nonlocality is both temporal and spatial, the latter given by a Biot-Savart interaction between segments of the interface. This form of coupling reminds us that the supercurrents that provide the screening of the applied magnetic field flow along the SN interfaces. Many years ago Pearl[14] and later Fetter and Hohenberg[15] showed that the interactions between currents flowing in thin slabs are long ranged. Thus vortices in a thin film interact with a potential whose long-range form is unscreened, $V(r)\sim 1/r$, while at short distances $V(r)\sim\ln(\Lambda/r)$, where Λ is a cutoff. Screening is unimportant at long distances because the interaction energy is dominated by the electromagnetic fields (*in vacuo*) above and below the slab.

Based on these observations, we proposed recently[16] a ''current-loop'' (CL) model as an approximate description of the intermediate state. The model treats the patterns as a collection of tense current ribbons, interacting with the Biot-Savart force of currents in free space and subject to global flux conservation. It is based on several simplifying assumptions. First, the domain walls are taken to be vertical, rather than flared as in Landau's calculation. Second, only supercurrents in those walls are considered: Surface supercurrents on the slab top and bottom are ignored. These approximations allow for an averaging process over the slab thickness that maps the model onto one of self-interacting contours in the plane. Such free-boundary approaches are well known for hydrodynamic problems such as Saffman-Taylor fingering,[17] as well as in reaction-diffusion systems.

While important phenomena such as domain fission are precluded in this model, it has the virtue of providing a simple picture of the mechanism of shape instabilities in this system and a useful starting point for a more precise treatment.[18] It is strikingly similar to models of interfacial pattern formation in a variety of other systems that display ''labyrinthine'' patterns from a competition between interfacial tension and electromagnetic interactions.[19] These include magnetic fluids,[20–24] Langmuir monolayers,[25–27] and thin magnetic films.[28] It is also related to a reaction-diffusion system[29–32] in which *chemical fronts* between two locally stable states form disordered labyrinths like those seen in gel reactors.[33,34]

In Sec. II we set the stage for a macroscopic model of the intermediate state by recalling both the sharp-interface limit of the time-dependent Ginzburg-Landau (TDGL) model for nonequilibrium superconductivity and the derivation of long-range interactions between currents in the slab geometry. The conformal mapping solution to Landau's model of the intermediate state and the simpler *straight-lamina* model are derived in Sec. III, with careful attention paid to the consequences of those long-range interactions. The free energy in the two models is shown to be essentially equivalent, as are their predictions for the equilibrium stripe width. The current-loop model is described and applied to the laminar state in Sec. IV, while instabilities of single flux stripes and the elastic properties of the laminar state are found in Sec. V. Section VI summarizes the experimental predictions and open issues.

II. PROPERTIES OF THE MACROSCOPIC MODEL

A. The sharp-interface limit

The microscopic parameters in the TDGL model include the charge e^* and mass m of a Cooper pair, a dimensionless order parameter relaxation time γ, and the conductivity σ of the normal phase. The equations of motion for the order parameter ψ and the scalar and magnetic vector potentials, ϕ and $\mathbf{A}$ are

$$\hbar\gamma\left(\partial_t+\frac{ie^*}{\hbar}\phi\right)\psi=\frac{\hbar^2}{2m}\left(\nabla-\frac{ie^*}{\hbar}\mathbf{A}\right)^2\psi+a\psi-b|\psi|^2\psi, \tag{2.1}$$

$$\nabla\times\nabla\times\mathbf{A}=4\pi(\mathbf{J}_n+\mathbf{J}_s), \tag{2.2}$$

where $\mathbf{J}_n$ and $\mathbf{J}_s$ are the normal and supercurrents

$$\mathbf{J}_n=\sigma(-\nabla\phi-\partial_t\mathbf{A}),$$

$$\mathbf{J}_s=\frac{\hbar e^*}{2mi}(\psi^*\nabla\psi-\psi\nabla\psi^*)-\frac{e^{*2}}{m}|\psi|^2\mathbf{A}. \tag{2.3}$$

The parameter $a=a_0(1-T/T_c)$ controls the correlation length $\xi=\hbar/(2m|a|)^{1/2}$ and penetration depth $\lambda=[mb/4\pi e^{*2}|a|]^{1/2}$. When ξ is small the SN interface is sharp; the inverse distance from the critical point measures that smallness. Setting $a=\tilde{a}/\epsilon^2$ and rescaling distances and fields with powers of ϵ, one finds that both λ and ξ scale identically. The sharp-interface limit is then $\xi,\lambda\to 0$ with $\kappa\equiv\lambda/\xi$ fixed, distinguishing between type-I ($\kappa<1/\sqrt{2}$) and type-II ($\kappa>1/\sqrt{2}$) systems.

Derivations of interface motion in this context presume translational invariance along the direction of the field and so describe ''bulk'' superconductors.[13] They show that far from the interface (the ''outer'' solution), the magnetic field in normal regions diffuses,

$$\mathbf{h}_t=D\nabla^2\mathbf{h}, \tag{2.4}$$

with $D=1/4\pi\sigma$. The boundary condition on the magnitude h_i of $\mathbf{h}$ on the interface $\mathcal{C}$ is

$$h|_{\mathcal{C}}=H_c\left[1-\frac{4\pi}{H_c^2}(\sigma_{\rm SN}\mathcal{K}+\Gamma^{-1}v_n)\right], \tag{2.5}$$

where $\sigma_{\rm SN}$ is the interfacial tension, $\mathcal{K}$ is the interface curvature, Γ is a kinetic coefficient, and $v_n=\hat{\mathbf{n}}\cdot\mathbf{r}_t$ is the normal component of the interface velocity.

The equation of motion expressing v_n in terms of $\mathbf{r}(s,t)$ follows from a solution to the diffusion equation (2.4) given Eq. (2.5) as a convolution over past times and all space. When $D\to\infty$ (vanishing normal state conductivity), the temporal nonlocality disappears, yielding

$$\Gamma^{-1}\hat{\mathbf{n}}\cdot\mathbf{r}_t(s,t)=\frac{H_c^2-H_a^2}{8\pi}+\sigma_{\rm SN}\mathcal{K}-\frac{H_c^2}{8\pi^2}\oint ds'\,\frac{\mathbf{R}\times\hat{\mathbf{t}}(s')}{R^2}, \tag{2.6}$$

with $\mathbf{R}=\mathbf{r}(s)-\mathbf{r}(s')$. Equation (2.6) has the variational form

$$\mathbf{r}_t=-\Gamma\frac{1}{\sqrt{g}}\frac{\delta\mathcal{H}_{\rm eff}}{\delta\mathbf{r}}, \tag{2.7}$$

where g is the interface metric and the effective interface Hamiltonian for a single domain is

$$\mathcal{H}_{\rm eff}[\mathbf{r}]=-\frac{H_c^2-H_a^2}{8\pi}A+\sigma_{\rm SN}L-\frac{H_c^2}{8\pi}\oint ds\oint ds'\hat{\mathbf{t}}(s)\cdot\hat{\mathbf{t}}(s')\mathcal{G}(R), \tag{2.8}$$

with terms proportional to the domain area A, from the field and condensation energy, and perimeter L, from the surface tension, while the distortion energy of the field lines is the self-induction of the boundary, with $\mathcal{G}(R)=-(1/2\pi)\ln R$ the Green's function of the two-dimensional Laplacian.

A temporally local but spatially nonlocal contour dynamics appears as well in a simpler reaction-diffusion system of recent interest.[29–32] This is the FitzHugh-Nagumo model[35] of the coupled dynamics of an activator u and inhibitor v in two spatial dimensions

$$u_t=\overline{D}\nabla^2u-F'(u)-\rho(v-u),$$

$$\epsilon v_t=\nabla^2v-v+u. \tag{2.9}$$

These partial differential equations are written in a rescaled form in which the activator diffusion constant $\overline{D}$ is normalized to that of the inhibitor, while ϵ is a ratio of their characteristic times. The function $F(u)$, whose derivative $F'(u)$ appears, is a double-well potential that describes the autocatalytic bistability of the activator. When $\epsilon\neq 0$, the coupled dynamics is not a gradient flow in any standard form.

The two systems (2.2) and (2.9) share many features. In each case there is a field (ψ or u) with an underlying bifurcation (continuous for ψ, first order for u), coupled to a diffusing field (unscreened or screened). In the superconductor, the second field can be integrated out in exchange for an instantaneous nonlocal coupling of the field ψ. An identical feature appears in the reaction-diffusion problem when the parameter ϵ is small, for then the inhibitor relaxes on times short compared to that of the activator and is slaved to u. Setting $\epsilon v_t=0$, the field inhibitor is $v=\int\mathcal{G}u$, with $\mathcal{G}$ the Green's function for the modified Helmholtz operator. This produces a nonlocal variational dynamics for u, $u_t=-\delta\mathcal{E}/\delta u$, with

$$\mathcal{E}[u]=\int d^2x\left\{\frac{1}{2}\overline{D}|\nabla u|^2+F(u)-\frac{1}{2}\rho^2\right\}+\frac{1}{2}\rho\int d^2x\int d^2x'u(\mathbf{x})\mathcal{G}(|\mathbf{x}-\mathbf{x}'|)u(\mathbf{x}'). \tag{2.10}$$

In the limit $\overline{D}\to 0$ Eq. (2.10) reduces to a functional of the contours bounding regions in which u takes on values corresponding to the minima of F. That functional of the position vectors $\mathbf{r}_i(s)$ of domain boundaries is[29,30]

$$\Delta\mathcal{E}[\{\mathbf{r}_i\}]=\overline{\gamma}\sum_i L_i+\Delta F\sum_i A_i-\frac{\rho}{2}\sum_{i,j}\oint ds\oint ds'\hat{\mathbf{t}}_i\cdot\hat{\mathbf{t}}_j\mathcal{G}(|\mathbf{r}_i-\mathbf{r}_j|), \tag{2.11}$$

with $\overline{\gamma}$ the line tension and L_i and A_i the domain perimeter and enclosed area. The nonlocal term is again the self- and mutual-induction of (here fictitious) currents.

B. Long-range forces

As further motivation for the CL model, we recall Pearl's derivation[14] of the unscreened potential between point vortices in a thin film. The starting point is the supercurrent surrounding a single vortex at the origin. The order parameter has the simple form

$$\psi(\mathbf{r})=\psi_0 f(r)e^{i\theta} \quad (0\leqslant z\leqslant d), \tag{2.12}$$

where ψ_0 is the far-field value of ψ, which vanishes for $z<0$ and $z>d$. The function $f(r)$ describes the vortex core structure and we take $f=1$ on the (large) scales of interest. The second Ginzburg-Landau equation is

$$\boldsymbol{\nabla}\times\boldsymbol{\nabla}\times\mathbf{A}=4\pi\mathbf{J}_s=\frac{1}{\lambda^2}\left[\frac{\psi_0}{2\pi r}\,\hat{\theta}-\mathbf{A}\right]. \tag{2.13}$$

If the film is sufficiently thin, then we may average over the film thickness d to obtain

$$\boldsymbol{\nabla}\times\boldsymbol{\nabla}\times\mathbf{A}=\frac{d}{\lambda^2}\left[\frac{\psi_0}{2\pi r}\,\hat{\theta}-\mathbf{A}\right]\delta(z). \tag{2.14}$$

In this form, it is readily apparent from the appearance of the term $-(d\mathbf{A}/\lambda^2)\delta(z)$ on the right-hand side that the screening is confined solely to the slab.

The solution to this can be obtained through the use of Fourier-Hankel transforms and yields the supercurrent

$$\mathbf{J}_s(r)=-\frac{\phi_0}{8\pi\Lambda^2}\left[H_1(r/\Lambda)-Y_1(r/\Lambda)-\frac{2}{\pi}\right]\hat{\theta}, \tag{2.15}$$

where H_1 and Y_1 are Hankel functions and the penetration depth for the thin film is $\Lambda=2\lambda^2/d$. The interaction potential of a point vortex a distance r from the first is obtained by multiplying Eq. (2.15) by ϕ_0 and integrating,

$$V(r)=\frac{\phi_0^2}{8\pi\Lambda}[H_0(r/\Lambda)-Y_0(r/\Lambda)]. \tag{2.16}$$

At distances $r/\Lambda\gg 1$, this is an unscreened potential

$$V(r)\simeq\frac{\phi_0^2}{4\pi^2 r}, \tag{2.17}$$

whereas as $r\to 0$ the familiar logarithmic interaction between vortices appears,

$$V(r)\simeq\frac{\phi_0^2}{4\pi^2\Lambda}\ln\left(\frac{e^C r}{2\Lambda}\right), \tag{2.18}$$

with C being Euler's constant. We anticipate therefore that the interactions between Meissner currents in a thin type-I slab should have a similar long-range character.

III. THE LAMINAR STATE

A. Landau's free-boundary solution

First, we calculate the shape and optimal spacing for an assumed laminar geometry for the intermediate state. While our work reproduces Landau's original calculation,[7] the method is quite different and provides an explicit expression for the function $f(h)$ (see below). We include this material in part to clarify this derivation but more importantly this ''exact'' result, for flared normal laminae, can be compared to simpler models of straight laminae and used as a test of the current-loop model.

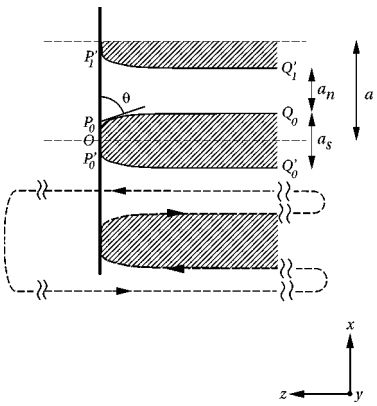

FIG. 3. Laminae in the intermediate state. Superconducting regions are shaded. Reference points P_n, Q_n, P_n', etc., are discussed in the text. The dashed line shows the contour used for the energy calculation.

In the semi-infinite geometry considered here (Fig. 3) the sample occupies the region $z<0$ with its surface in the x-y plane. The applied field is perpendicular to the sample, $\mathbf{H}_a=H_a\hat{z}$, producing an array of normal-superconducting laminae periodic in the x direction, and straight along $\hat{y}$. The normal and superconducting laminae have asymptotic widths a_n and a_s, respectively, so the period of the entire structure is $a=a_s+a_n$.

Since the SN interfaces are sharp compared to the lamina spacing we work with the macroscopic Maxwell equations. In the normal regions $\boldsymbol{\nabla}\times\mathbf{B}=0$ and $\boldsymbol{\nabla}\cdot\mathbf{B}=0$, which can be solved by introducing either the scalar potential ϕ through $\mathbf{B}=-\boldsymbol{\nabla}\phi$, so that $\nabla^2\phi=0$, or the vector potential $\mathbf{A}$ through $\mathbf{B}=\boldsymbol{\nabla}\times\mathbf{A}$, which in the gauge $\nabla\cdot\mathbf{A}=0$ satisfies $\nabla^2\mathbf{A}=0$. To solve this Laplace equation in the x-z plane, we use complex variable methods; for the laminar structure the only nonzero component of the vector potential is A_y and we introduce the complex potential $w=\phi+i\psi=\phi+iA_y$ so that the complex magnetic field is

$$B=B_x-iB_z=-\frac{dw}{d\zeta}, \quad \zeta=x+iz. \tag{3.1}$$

The boundary condition as $z\to\infty$ is that the field becomes the uniform applied field $H_a\hat{z}$, so $w\to iH_a\zeta$. Since the magnetic field vanishes in the superconducting regions, continuity of its normal component implies that the field is purely tangential both along the normal-superconducting interface P_nQ_n and the ''nose'' OP_n (Fig. 3). In the first case, the assumption of thermodynamic equilibrium at this interface implies that the magnitude H_n of the tangential component is a constant (as yet unknown), so that the vector potential A_y is also constant along any one interface. Along the nose the magnetic field is parallel to the surface ($\mathbf{H}=H_x\hat{x}$) but with a varying magnitude. The field H_n and the periods a_n and a_s are determined *a posteriori* by minimizing the energy. They are constrained by flux conservation, $H_a a=H_n a_n$, so for fixed external field H_a the energy is determined by a and a_n.

TABLE I. Analogies between free streamline flow in fluids and lamina formation in the intermediate state of type-I superconductors.

Free streamline flow around a plate	Laminae in superconductors
complex potential $w=\phi+i\psi$	complex potential $w=\phi+iA_y$
complex fluid velocity $u-iv=-dw/d\zeta$	complex magnetic field $B=B_x-iB_z=-dw/d\zeta$
streamlines	field lines (lines of force)
free streamline	superconducting-normal interface
free streamline velocity U	superconducting critical field H_c
region of fluid flow	normal phase with nonzero magnetic field
cavity behind plate	superconducting phase
Riabouchinsky flow	lamina in a finite thickness plate

1. Exact determination of the lamina shape

The position of the SN interface is not known *a priori* and must be discovered in the process of solving the problem. This seemingly formidable task is simplified by recognizing that our magnetostatics problem is formally equivalent to the flow of an ideal incompressible fluid around an array of plates, the plates being the noses of the laminae. The field lines would be the fluid streamlines; the SN interfaces correspond to ''free streamlines'' that have separated from the flow behind the plate. The full correspondence is given in Table I. The shape of the free streamlines can be determined by using the *hodograph method*,[36,37] which recognizes that while the field lines in the ζ plane may be complicated, the field configuration in the w and H planes is quite simple; a conformal transformation mapping the w plane onto the H plane leads to a relation between w and $dw/d\zeta$, the solution of which determines the interface shape. Consider first the w plane. Since the magnetic field is tangent to both the nose segment and to the SN interface, the magnitude of the vector potential is constant on these segments, as well as on the centerline shown dashed in Fig. 3. Far from the sample (at a fixed $z\to\infty$), $A_y\sim H_a x$; therefore, for laminae separated by a distance a, the vector potential on the interface of the nth lamina is $A_y=H_a n a$. The potential ϕ behaves as $-zH_a$ as $z\to\infty$, hence the laminae correspond to the positive half of the ϕ axis. Figure 4(a) shows the field configuration in the w plane. Next we consider the H plane and introduce the normalized magnetic field

$$\eta=\frac{H}{H_n}=-\frac{1}{H_n}\frac{dw}{d\zeta}. \tag{3.2}$$

On the interface $|\eta|=1$, and so set $\eta=-e^{-i\theta}$, where θ, the tangent angle (as in Fig. 3), changes as we traverse the interface from the point P_n to Q_n; this produces a semicircle in the η plane. On the nose $\eta_x=0$, so the segment $P_n'P_n$ maps onto a horizontal straight line in the η plane. Therefore, the region *exterior* to the superconducting laminae maps onto the *interior* of a semicircle, as shown in Fig. 5(a) (the *hodograph* for the field).

The map from the w plane onto the η plane is most easily carried out by first taking care of the periodicity in the w plane by mapping it onto the σ plane with the transformation $\sigma=\exp(2\pi w/H_a a)-1$, so that the σ plane has a single cut along the positive real axis [Fig. 4(b)]. Next, map the σ plane onto the lower half of the λ plane with $\lambda=(k^2/\sigma)^{1/2}$ [Fig. 5(b)], where k is set by boundary conditions. Finally, map the η plane onto the λ plane using the Joukowsky transformation $\lambda=(1/\eta+\eta)/2$. To determine k, we notice that as $z\to\infty$, $w\to-\infty$, so that $\sigma=-1$ and $\eta=H_a/H_n$. Defining $h_a\equiv H_a/H_n$, we have $k^2=(1-h_a^2)^2/4h_a^2$.

These transformations yield the complex potential

$$w=\frac{H_a a}{2\pi}\ln\left[\frac{(\eta^2+h_a^2)(\eta^2+h_a^{-2})}{(1+\eta^2)^2}\right]. \tag{3.3}$$

The shape of the lamina is found using Eq. (3.2),

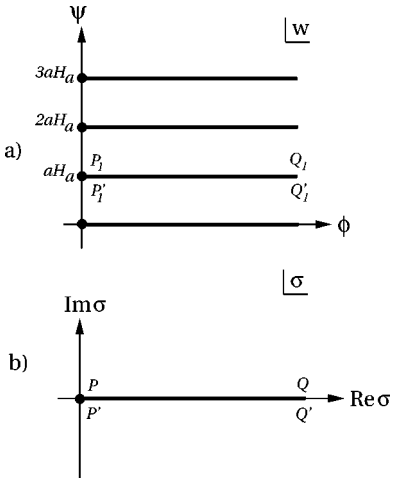

FIG. 4. w and σ planes.

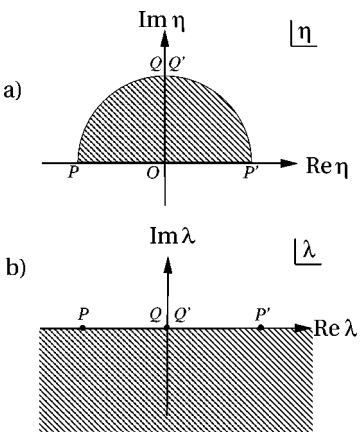

FIG. 5. η and λ planes.

$$\frac{d\zeta}{d\eta}=\frac{d\zeta}{dw}\frac{dw}{d\eta}=-\frac{1}{H_n}\frac{1}{\eta}\frac{dw(\eta)}{d\eta}$$
$$=-\frac{a}{\pi}\frac{(1-h_a^2)^2}{h_a}\frac{1-\eta^2}{(\eta^2+h_a^{-2})(\eta^2+h_a^2)(\eta^2+1)}. \tag{3.4}$$

Integrating by a partial fraction expansion and fixing an integration constant with $\eta(z=0)=0$, we have

$$\zeta(\eta)=-\frac{iah_a}{\pi}\left[\frac{1}{2h_a}\ln\left(\frac{h_a-i\eta}{h_a+i\eta}\right)+\frac{h_a}{2}\ln\left(\frac{h_a^{-1}-i\eta}{h_a^{-1}+i\eta}\right)\right.$$
$$\left.-\ln\left(\frac{1-i\eta}{1+i\eta}\right)\right], \tag{3.5}$$

which implicitly determines the magnetic field η as a function of position ζ. Though this parametrization differs from Landau's,[7,38] it is equivalent to and coincides with that of Fortini and Paumier,[39] although the method of derivation is entirely different. The equivalent fluid problem is separated flow past a plate placed symmetrically in a channel, whose solution [Ref. 37, p. 39, Eq. (25a)] is Eq. (3.5) above.

To calculate the lamina shape, recall the relation $\eta=-e^{-i\theta}$ on the SN interface. Substituting into Eq. (3.5), we obtain after a great deal of algebra two parametric equations for the interface position:

$$x(\theta)=\frac{a}{2}\left[1-h_a-\frac{(1-h_a^2)}{\pi}\tan^{-1}\left(\frac{2h_a\cos\theta}{1-h_a^2}\right)\right],$$

$$z(\theta)=\frac{a}{4\pi}\left[(1+h_a^2)\ln\left(\frac{1+h_a^2+2h_a\sin\theta}{1+h_a^2-2h_a\sin\theta}\right)\right.$$
$$\left.-4h_a\ln\left(\frac{\cos\theta}{1-\sin\theta}\right)\right]. \tag{3.6}$$

The width $2b$ of the nose can now be determined from Eq. (3.6) by setting $\theta=0$, with the result

$$b=\frac{a}{2}(1-h_a)-\frac{a}{2\pi}(1-h_a^2)\sin^{-1}(2h_a/1+h_a^2). \tag{3.7}$$

Lamina shapes calculated from Eq. (3.6) at different applied fields h_a are shown in Fig. 6.

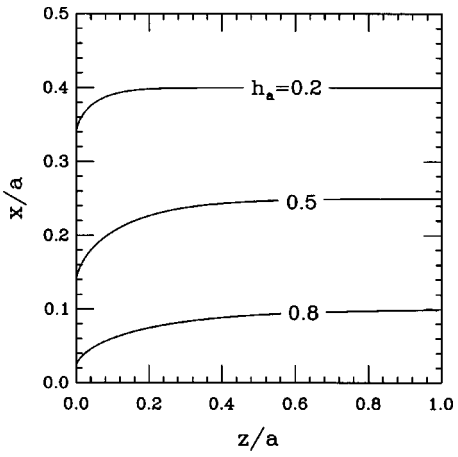

FIG. 6. Lamina shapes calculated from Eq. (3.6).

2. Energy of the laminar structure

The total free energy of the laminar state has contributions from the condensation energy, the magnetic field, and the SN interfaces. The first is $-H_c^2/8\pi$ times the volume occupied by the superconducting phase. If the SN interfaces did not bend at all, this energy would be $-(H_c^2/8\pi)(Na_s)L_yd$, with N the total number of laminae and L_y the length of the sample in the y direction [note that the sample has a total area $A=(Na)L_y$]. To this we add the condensation energy lost from the thinning of superconducting regions near the slab surfaces, obtaining

$$\frac{E_c}{A}=-\frac{H_c^2d}{8\pi}\frac{a_s}{a}+\frac{4}{a}\frac{H_c^2}{8\pi}\int_{-\infty}^{0}\left[\frac{a_s}{2}-x(z)\right]dz, \tag{3.8}$$

the factor of 4 in front of the integral accounting for the four corners of the lamina. The integral is

$$\int_{-\infty}^{0}\left[\frac{a_s}{2}-x(z)\right]dz=-\int_0^{\pi/2}\left[\frac{a_s}{2}-x(\theta)\right]\frac{dz}{d\theta}\,d\theta$$
$$=\frac{a^2h_a(1-h_a^2)}{2\pi^2}\int_0^{\pi/2}d\theta$$
$$\times\frac{\tan^{-1}(p\cos\theta)(1-\cos^2\theta)}{\cos\theta(1+p^2\cos^2\theta)}, \tag{3.9}$$

where $p=2h_a/(1-h_a^2)$ and the second line was obtained with Eq. (3.6). A partial fraction expansion and integrations by parts reduce the integral in Eq. (3.9) to $(\pi/2)[\ln(p+q)-(q/p)\ln q]$, with $q=(1+p^2)^{1/2}$. The condensation energy is then

$$\frac{E_c}{A}=-\frac{H_c^2d}{8\pi}+\frac{H_c^2d}{8\pi}\left[\frac{a_n}{a}+\frac{a}{d}f_c(h_a)\right], \tag{3.10}$$

with

$$f_c(h)=\frac{1-h^2}{2\pi}[(1+h)^2\ln(1+h)+(1-h)^2\ln(1-h)$$
$$-(1+h^2)\ln(1+h^2)]. \tag{3.11}$$

The magnetic field energy is found by integrating $B^2/8\pi$ over the space inside and outside the sample. For our periodic structure this energy per unit area is

$$\frac{E_m}{A}=\frac{2}{a}\int_{\mathcal{C}}\frac{B^2}{8\pi}\,dxdz, \tag{3.12}$$

where the factor of 2 accounts for the top and bottom surfaces of the sample and the integral is over the area $\mathcal{C}$ of one cell (Fig. 3). In this two-dimensional geometry $B^2=(\nabla A_y)^2$, and with $\nabla^2A_y=0$ Eq. (3.12) becomes a line integral around the unit cell boundary $\partial\mathcal{C}$:

$$\frac{E_m}{A}=\frac{2}{8\pi a}\int_{\partial\mathcal{C}}A_y(s)B_s(s)\,ds, \tag{3.13}$$

with $A_y(s)$ the vector potential on the boundary and $B_s(s)$ the tangential component of the magnetic field.

The advantage of this representation of the field energy is that the vector potential is *constant* on the boundaries and can therefore be brought outside the integral. Let us consider the various contributions to the integral. On the SN interface (segments $Q'P'$ and PQ) the integral $\int B_s ds$ vanishes, as the field points in the same direction on the left and right halves of the superconducting lamina. On the midline between laminae $n-1$ and n, the vector potential is $H_a a(n-1)/2$, while on the next midline up it is $H_a(n+1)/2$; the integral $\int B_s ds$ is equal in magnitude but opposite in sign for these two segments since the integration paths are in opposite directions. Adding these two contributions and using $B_s = -\partial\phi/\partial s$ we have

$$\frac{E_m}{A} = \frac{H_a}{4\pi}[\phi(a/2,-d/2) - \phi(a/2,L_z/2)], \qquad (3.14)$$

where L_z is some large distance away from the top surface of the sample. The entire calculation of the field energy then reduces to finding the asymptotic behavior of the scalar potential along one of the streamlines (the midline, in this case). Examining the behavior of Eq. (3.3) for the complex potential w and Eq. (3.5) for the position ζ, as $\eta \to 1$ and $\eta \to h_a$, we find the asymptotic behavior $\phi(a/2,L_z/2) \sim -H_a L_z/2 - (H_a a/2\pi)\phi_+$, where

$$\phi_+ = \ln 4 + (1+h_a^2)\ln(1+h_a^2) - (1+h_a)^2 \ln(1+h_a) - (1-h_a)^2 \ln(1-h_a), \qquad (3.15)$$

and $\phi(a/2,-d/2) \sim -H_n a/2 - (H_n a/2\pi)\phi_-$, where

$$\phi_- = (1-h_a)^2 \ln(1-h_a) + 2h_a \ln 4h_a - (1+h_a)^2 \ln(1+h_a). \qquad (3.16)$$

Substituting into Eq. (3.14), we have

$$\frac{E_m}{A} = \frac{H_a^2}{8\pi} L_z + \frac{H_n H_a}{8\pi} d + \frac{H_n^2}{4\pi} a f_{\rm mag}(h_a), \qquad (3.17)$$

with

$$f_{\rm mag}(h_a) = \frac{h_a}{2\pi}[(1+h_a)^3 \ln(1+h_a) - 2h_a \ln 8h_a - (1-h_a)^3 \ln(1-h_a) - h_a(1+h_a^2)\ln(1+h_a^2)]. \qquad (3.18)$$

The first term in Eq. (3.17) is the energy of the external field in the absence of the sample, which is of no interest and henceforth neglected. The second term is the bulk magnetic field energy of a uniformly magnetized sample[40] and the third arises from demagnetizing fields (due to the partitioning of the sample into domains).

Finally, we calculate the surface energy. If $\sigma_{\rm SN}$ is the surface tension, then the energy for a single interface is $\sigma_{\rm SN} dL_y$.[41] Since there are two interfaces per lamina and N laminae in the sample, the total interfacial energy is $2\sigma_{\rm SN} dL_y N = 2\sigma_{\rm SN} A(d/a)$. Introducing the length Δ, essentially the width of the interfaces, through $\sigma_{\rm SN} = (H_c^2/8\pi)\Delta$, the interfacial energy per unit area is

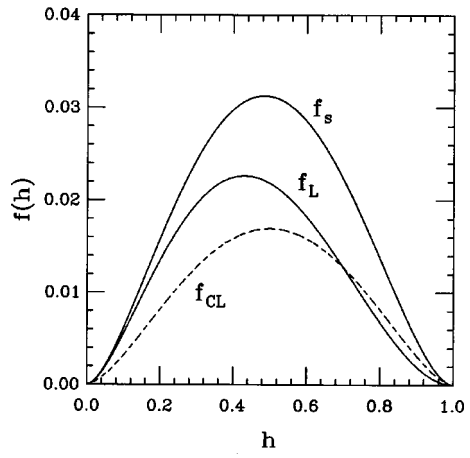

FIG. 7. Functions $f_L(h)$ in Landau's model, $f_s(h)$ in the straight-lamina approximation, and $f_{\rm CL}(h)$ from the current-loop model.

$$\frac{E_{\rm int}}{A} = \frac{H_c^2}{8\pi}\frac{2\Delta d}{a}. \qquad (3.19)$$

Summing the contributions (3.10), (3.17), and (3.19) and using flux conservation, we find

$$\frac{E}{A} = \frac{H_c^2 d}{8\pi}\left\{ -1 + \left[\frac{a_n}{a} + h^2\frac{a}{a_n}\right] + 2\left(\frac{\Delta}{a} + \frac{a}{d}\left[2 f_c(h_a) + \frac{H_n^2}{H_c^2} f_{\rm mag}(h_a)\right]\right)\right\}, \qquad (3.20)$$

with $h \equiv H_a/H_c$. Minimizing this with respect to both a and a_n results in very cumbersome expressions. Instead, we minimize the first term in brackets with respect to a_n, which yields $a_n = ha$, so that $H_n = H_c$ (and $h_a = h$). This is the result used by Landau and is reasonably accurate as long as the surface and demagnetizing energies are small. Substituting back into the energy, we obtain

$$\frac{E}{A} = -\frac{H_c^2 d}{8\pi} + \frac{H_c H_a d}{4\pi} + \frac{H_c^2 d}{4\pi}\left[\frac{\Delta}{a} + \frac{a}{d} f_L(h)\right], \qquad (3.21)$$

with

$$f_L(h) = 2 f_c(h) + f_{\rm mag}(h) = \frac{1}{4\pi}[(1+h)^4 \ln(1+h) + (1-h)^4 \ln(1-h) - (1+h^2)^2 \ln(1+h^2) - 4h^2 \ln 8h]. \qquad (3.22)$$

This function is plotted in Fig. 7. Its asymptotic behavior as $h \to 0$ is of interest in comparison with other approaches and has the form $f_L(h) \simeq (h^2/\pi)\ln(0.56/h)$. Finally, the equilibrium laminar period is obtained simply by minimizing with respect to a, yielding

$$a^* = \left[\frac{\Delta d}{f(h)}\right]^{1/2}. \qquad (3.23)$$

This implies that the spacing diverges for small h as

$$a^* \simeq \frac{(\Delta d)^{1/2}}{h}\left[\frac{\pi}{\ln(0.56/h)}\right]^{1/2}. \tag{3.24}$$

B. Energy of a straight-lamina model

It is useful to compare the results from the Landau model to an alternative *straight-lamina model*, in which the segments P_nQ_n of Fig. 3 are made straight. In this model the field is still tangent to the SN interface, but the magnitude of the field is not constant along the interface. The field and the complex potential can be obtained using standard conformal mapping methods; the problem is equivalent to an ideal fluid flowing in a channel with an abrupt step.[36] The solution is

$$w = \frac{H_a a}{2\pi}\ln\left(\frac{\eta^2+1}{\eta^2+h_a^2}\right), \tag{3.25}$$

$$\zeta = \frac{a_s}{2} + \frac{iah_a}{2\pi}\left[\ln\left(\frac{\eta+i}{\eta-i}\right) - \frac{1}{h_a}\ln\left(\frac{\eta+ih_a}{\eta-ih_a}\right)\right].$$

Under the simplifying assumption that $H_n = H_c$, the total energy in this model is

$$\frac{E}{A} = -\frac{H_c^2 d}{8\pi} + \frac{H_c H_a d}{4\pi} + \frac{H_c^2 d}{4\pi}\left[\frac{\Delta}{a} + \frac{a}{d}\, f_s(h)\right], \tag{3.26}$$

with

$$f_s(h) = \frac{h}{2\pi}[(1+h)^2\,\ln(1+h) - (1-h)^2\,\ln(1-h) - 2h\,\ln 4h]. \tag{3.27}$$

This function is plotted in Fig. 7 for comparison with Landau's result (3.22). At small h it behaves as $f_s(h) \simeq (h^2/\pi)\ln(0.68/h)$, very close to $f_L(h)$. The total energy (3.26) has the same qualitative dependence upon the lamina spacing a as the Landau model, although the latter has lower energy for any reduced field h.

C. Lamina shapes in finite-thickness plates

In the analyses above we assumed that the superconductor slab is sufficiently thick that the shapes of the lamina walls can be computed as for a semi-infinite slab. When the thickness d becomes small enough the wall shapes will change. From the asymptotic behavior of the semi-infinite solutions (3.6), we deduce that the thickness approaches its asymptotic values for $z \to -\infty$ as

$$\frac{a}{2}(1-h_a) - x(z) \sim \frac{4h_a}{\pi}\exp(\pi z/ah_a). \tag{3.28}$$

The decay length ah_a/π should then determine when finite-slab thickness effects become important. The asymptotic results show that the product ah vanishes very slowly (logarithmically) as $h \to 0$, so that while such finite-thickness effects become important in that limit, practically the relevant fields are very small. The crossover field h_x for $ah_a/\pi = d$ is on the order of $h_x \sim 0.56\exp(-\Delta/\pi d)$. For $h \leqslant h_x$ the slab thickness has no significant effect on the domain wall shapes. In the fluid dynamical analogy, the finite-thickness calculation is equivalent to Riabouchinsky flows around *two* plates, the details of which are found in standard references.[37]

IV. THE CURRENT-LOOP MODEL

The analysis above of the laminar state shows that in accounting for the flaring of the normal domains Landau's free-boundary approach yields a lower-energy structure than a model with straight walls. However, the analytical and numerical differences between the two approaches are minor. In both models the supercurrents flow along the SN interfaces *and* on the top and bottom surfaces of the sample.[18,42] Just as the magnetic field in a solenoid is more uniform when it is a tall thin cylinder than when it is short and wide, so too the contributions from circulating currents along the SN interfaces should dominate when the flux domains are narrow and tall, at low fields. This suggests that the basic physics of the laminar state can be understood from those circulating currents alone. We now develop this current-loop model and show that it rather accurately reproduces the results of Landau's model, an important test of an approach that can easily be generalized to SN interfaces of arbitrary shape.

A. Energetics of the current-loop model

In this model, as above, the intermediate state is described in macroscopic terms, but now the SN interfaces encircling each of the normal regions belong to a set $\{\mathcal{D}_i\}$ each with area A_i and perimeter L_i. The two phases occupy volumes V_s and $V_n = d\Sigma_i A_i$, with $V_s + V_n = V$. Parametrizing each boundary by arclength, the position vectors of the interfaces are $\mathbf{r}_i(s)$. As in the straight-lamina model, $\mathbf{r}_i$ is assumed independent of z, neglecting the flaring of the domain walls near the film surfaces.

The total energy is $E[\{\mathbf{r}_i\}] = E_c + E_{\rm int} + E_m$, a sum of the condensation energy E_c, the interfacial energy $E_{\rm int}$, and the magnetic field energy E_m. As before,

$$E_c = V\frac{H_c^2}{8\pi}\rho_n, \quad E_{\rm int} = \frac{H_c^2}{8\pi}\Delta d\sum_i L_i, \tag{4.1}$$

where $\rho_n = A_n/A$ is the area fraction of the normal phase and E_c is measured with respect to the purely superconducting state. Flux conservation relates the field in the normal regions to the applied field, $H_n = H_a/\rho_n$, and by the tangential continuity of $\mathbf{H}$ across a SN interface the field in the superconducting region is $H_s = H_n$. The perfectly diamagnetic superconducting regions each have a magnetization $\mathbf{M} = -(H_n/4\pi)\hat{\mathbf{e}}_z$, related to the (Meissner) currents that flow along the SN (and top and bottom sample) boundaries.

We compute the magnetic field energy as a sum of two contributions, the first of which is that of the domain magnetizations $\mathbf{M}$ in the presence of the external field $(-\int d^3r\ \mathbf{H}_a\cdot\mathbf{M})$. The second is the self- and mutual induction of the current ribbons. Expressing these in terms of the macroscopic quantities ρ_n, etc., we have

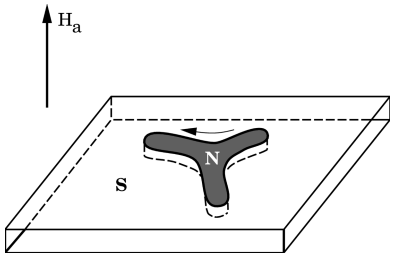

FIG. 8. Current loop.

$$E_m = V\frac{H_a H_n}{4\pi}(1-\rho_n) - \frac{1}{2}M^2\sum_{i,j}\int_0^d dz\int_0^d dz'\oint ds\oint ds'\frac{\hat{\mathbf{t}}_i\cdot\hat{\mathbf{t}}_j}{R_{ij}}, \tag{4.2}$$

where $M=-H_n/4\pi$. The unit tangent vectors $\hat{\mathbf{t}}_i(s)$ to the current ribbons label the direction of the current flow. By the usual screening processes in superconductors, the direction of the flow is so as to cancel the applied field in the superconducting regions and augment it in the normal regions (Fig. 8). Of course, the scalar product $\hat{\mathbf{t}}_i\cdot\hat{\mathbf{t}}_j$ is invariant under the overall reversal of the parametrizations ($s\to -s$). The free-space current-current interaction is Coulombic, with $R_{ij}=\{[\mathbf{r}_i(s)-\mathbf{r}_j(s')]^2+(z-z')^2\}^{1/2}$. Performing the z and z' integrals, the field energy becomes

$$E_m = V\frac{H_a H_n}{4\pi}(1-\rho_n) - M^2 d\sum_{i,j}\oint ds\oint ds'\hat{\mathbf{t}}_i\cdot\hat{\mathbf{t}}_j\Phi(R_{ij}/d), \tag{4.3}$$

where now the elementary free boundaries are *contours in the plane*, interacting with the potential

$$\Phi(R/d) = \frac{1}{2d}\int_0^d dz\int_0^d dz'[R^2+(z-z')^2]^{-1/2} = \sinh^{-1}(d/R)+R/d-\sqrt{1+(R/d)^2}, \tag{4.4}$$

where $R=|\mathbf{R}|$ with $\mathbf{R}(s,s')=\mathbf{r}(s)-\mathbf{r}(s')$ the in-plane vector between points labeled by s and s'. As discussed elsewhere,[23] this potential is Coulombic for $R\gg d$, $\Phi\approx d/2R$, but for $R\ll d$, $\Phi\approx\ln(2e^{-1}d/R)$, with the film thickness d acting as a cutoff. Note the interesting parallel with Pearl's vortex interaction potential (2.16) in thin films. The appearance of the potential Φ in the free-boundary approach to a number of other systems (see Table II) offers an explanation for the similarity in their behavior.

B. Current-loop description of the laminar state

Now we calculate the energy of the laminar state in the CL model, using the same geometrical quantities as before. The nonlocal magnetic contribution is the only difficult one. It proves convenient to return to the self-induction form of the current ribbons and to introduce a Fourier representation, which for a uniform laminar structure yields the magnetic field energy E_m per unit area

$$\frac{E_m}{A} = -\frac{M^2}{a}\sum_{n=-\infty}^{\infty}\int_{-\infty}^{\infty}dy\int_0^d dz\int_0^d dz' \times\int\frac{d^3q}{(2\pi)^3}\frac{4\pi}{q^2}e^{i[nq_x a+q_y y+q_z(z-z')]}(1-e^{iq_x a_n}). \tag{4.5}$$

Several straightforward integrations reduce this to

$$\frac{E_m}{A} = -\frac{aM^2}{\pi^2}\sum_{n=1}^{\infty}\frac{[1-\cos(2\pi n a_n/a)]}{n^3}\times\left(\frac{2\pi n d}{a}+e^{-2\pi d n/a}-1\right). \tag{4.6}$$

Note that the last term contains all of the d dependence of the sum. The leading contribution in the limit of large slab

TABLE II. Analogies between interfacial energetics of type-I superconductors and other systems. The energy of a set $\{\mathcal{D}_i\}$ of domains is written as $E[\{\mathbf{r}_i\}]=\Pi\Sigma_i A_i+\gamma\Sigma_i L_i-\frac{1}{2}\Omega\oint ds\oint ds'\hat{\mathbf{t}}_i\cdot\hat{\mathbf{t}}_j\Phi_{ij}(R_{ij}/\xi)$. The symbols denote the following: $\sigma_{\rm FW}$, ferrofluid water surface tension; M, ferrofluid magnetization; $\gamma_{\rm LE\text{-}LC}$, line tension between liquid expanded (LE) and liquid condensed (LC) phases in a Langmuir monolayer; $\Delta\mu$, discontinuity in electric dipole moment density between LE and LC phases; $d_{\rm mol}$, a molecular cutoff of monolayer thickness.

System	Π	γ	Ω	Φ	ξ
type-I superconductors[a]	$(H_c^2 d/8\pi)(\rho_n+h^2/\rho_n)$	$H_c^2 d\Delta/8\pi$	$H_n^2 d/8\pi^2$	$\sinh^{-1}(1/z)+z-\sqrt{1+z^2}$	d
magnetic fluids[b]	Lagrange multiplier	$d\sigma_{\rm FW}$	$2dM^2$	$\sinh^{-1}(1/z)+z-\sqrt{1+z^2}$	d
Langmuir monolayers[c]	Lagrange multiplier	$\gamma_{\rm LE\text{-}LC}$	$(\Delta\mu)^2$	$1/2z$[e]	$d_{\rm mol}$
FitzHugh-Nagumo model[d]	ΔF	$\overline{D}$	ρ	$K_0(z)$	1[f]

[a]Present work.
[b]References 23 and 24
[c]References 26 and 27.
[d]Equation (2.9) and Refs. 29 and 30.
[e]This limiting form is supplemented with a cutoff procedure. See Ref. 27.
[f]The system of units in Eq. (2.9) sets the inhibitor screening length equal to unity.

thickness is a ''bulk'' contribution expressible simply in terms of the stripe dimensions

$$\sum_{n=1}^{\infty} \frac{1-\cos(2\pi n a_n/a)}{n^2} = \pi^2 \frac{a_n(a-a_n)}{a^2}. \qquad (4.7)$$

It follows that the form of the free energy is like that in Eqs. (3.20) and (3.21), but with a new function f,

$$f_{\mathrm{CL}}(h,d,a) = \frac{1}{2\pi^3} \sum_{n=1}^{\infty} \frac{\sin^2(n\pi h)}{n^3} [1-e^{-2\pi n d/a}]. \qquad (4.8)$$

As in Landau's calculation, finite-thickness effects show up when d is comparable to a.

There are several noteworthy features of the function $f_{\mathrm{CL}}(h)$, particularly in the limit $d/a \gg 1$ considered here. First, as shown in Fig. 7, it is rather close to the Landau function and hence its implications for the equilibrium laminar thickness are in reasonable accord with experiment.[16] Second, it has the same structure as f_L as $h \to 0$, $f_{\mathrm{CL}}(h) \simeq (h^2/2\pi)\ln(0.71/h)$. Third, it has an *exact* symmetry under the transformation $h \to 1-h$, a reflection of the straight SN interfaces presumed in the model. This symmetry is absent in Landau's calculation and in the straight-lamina model by virtue of the currents on the slab faces. Finally, the form of the magnetic field energy in Eq. (4.6) is identical to the field energy of a stripe array in a thin ferromagnetic film.[43,44]

C. A dynamical model

The competition between surface tension and self-induction in the current-loop model appears in a number of other contexts (Table II), where it has been shown to produce also a rich dynamical behavior. While the precise connection between the Young-Laplace and Biot-Savart forces and the interface *dynamics* depends on the physical setting (e.g. Hele-Shaw flow with Darcy's law, surfactant monolayers with coupling to the fluid subphase, and reaction-diffusion systems), the phenomenon of branching instabilities producing disordered lamellar structures is ubiquitous. This suggests that much can be learned from the very simplest dynamical law for interface motion, the *local dissipation model*,[23] in which a local viscous force acting at the interface balances the pressure difference, expressed as a functional derivative (2.7).

A first step toward a full study of the *many-interface* current-loop model is the simplest mean-field description of a *single* current loop. That loop is assigned to a cell (analogous to a Wigner-Seitz cell) of area A_{cell} from which we compute the area fraction $\rho_n = A_n/A_{\mathrm{cell}}$. In this approximation, the self-induction of the loop is retained, but the mutual induction term in the energy associated with all other loops only contributes a bulk energy term like that in the laminar calculation (4.7). Moreover, the amplitude of the circulating currents is taken to be H_c rather than the actual local field, equivalent to assuming that the actual area fraction is near its equilibrium value. The system is then characterized by a single geometrical parameter $p \equiv 2R_{\mathrm{equiv}}/d$ describing the aspect ratio, where R_{equiv} is the radius of the circle whose area is that of the initial condition, and a single energetic parameter, the reduced magnetic field h. All other parameters simply rescale time.

In this model, the interface velocity is

$$\hat{\mathbf{n}} \cdot \mathbf{r}_t(s) = \frac{H_c^2 d}{8\pi\eta} \left\{ \Pi - \Delta \mathcal{K}(s) - \frac{1}{2\pi d} \oint ds' \hat{\mathbf{R}} \times \hat{\mathbf{t}}(s') \Psi(R/d) \right\}, \qquad (4.9)$$

with $\mathcal{K}(s)$ the curvature and $\Psi(\xi) = \Phi'(\xi) = 1-(1+\xi^{-2})^{1/2}$ the generalization of the Biot-Savart force to finite-thickness slabs.[23] The pressure term is

$$\Pi = h^2/\rho_n^2 - 1. \qquad (4.10)$$

The kinetic coefficient η may be estimated[13] from results on the bulk properties of strongly type-I systems,

$$\eta = \frac{H_c^2 d\Delta}{8\pi} \frac{\pi\hbar}{8k_B T_c \xi_0^2}, \qquad (4.11)$$

where again T_c is the critical temperature and ξ_0 is the bare correlation length.[45]

A contour dynamics such as Eq. (4.9) is readily generalized to account for surface tension anisotropy, a material feature that has long been suggested to play a role in the morphology of the intermediate state patterns,[1] as it does in problems such as dendritic growth.[46] When the anisotropy is q-fold, the parameter Δ has the form $\Delta = \Delta_0[1+\epsilon\cos(q\theta)]$. Typical experiments show a $q=4$ or $q=6$ anisotropy.[47] Our intuition suggests that the variation of σ_{SN} through Δ will bias instabilities toward q-fold symmetry and lead to preferred orientations of flux stripes produced from those instabilities.

D. Instabilities: Numerical studies

Two regular geometries of flux domains have historically been of interest: circles and stripes. In Sec. V we consider in detail the stability of stripes and stripe arrays; here we focus on fingering and branching instabilities of circular domains. Since linear stability analyses for circular interfaces have been presented in detail elsewhere in the context of closely related models,[22–24,26,27,30] we do not repeat them here. Two important qualitative results are that for a given domain radius and slab thickness (i) there exists a finite applied field above which azimuthal modes become active and (ii) instabilities of increasing mode number occur with ever larger applied field. Numerical studies of the contour dynamics illustrate these properties and allow us to see the highly nonlinear regime far beyond the instabilities.

An efficient numerical method for studying this nonlocal interface dynamics has been described in detail elsewhere.[27,30] It uses pseudospectral techniques to solve for the time evolution of the local tangent angle $\theta(s)$, from which the $[x(s),y(s)]$ coordinates of the interface are computed by basic differential geometry. For the purposes of verifying the analytical stability results as well as investigating such phenomena as mode competition, the initial contour is given a curvature $\mathcal{K}$ perturbed from that of a circle,

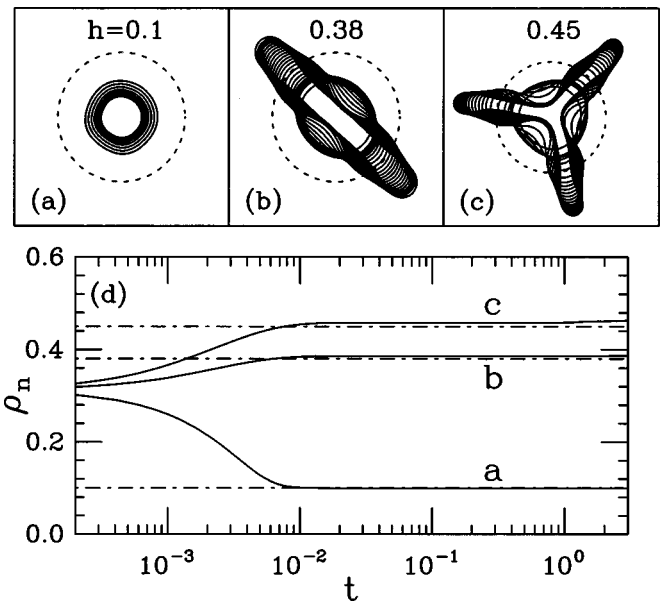

FIG. 9. Numerical studies of the current-loop model at aspect ratio $p=5.0$. Dashed circles in (a)–(c) indicate the unit cell. (a) Stable relaxation of a nearly circular initial condition to a circle of smaller radius, (b) elongational instability of a circular flux domain, (c) branching instability, and (d) time evolution of the normal area fraction ρ_n for cases (a)–(c). Dashed lines indicate the relation $\rho_n=h$ determined by the bulk energetic contributions alone.

$\mathcal{K}(\alpha)=1/R_0+\Sigma_{n=2}[a_n\cos(n\alpha)+b_n\sin(n\alpha)]$, where R_0 is the unperturbed radius and $\alpha=s/R_0$.

Figure 9 shows three basic phenomena described by the contour dynamics. The first [Fig. 9(a)], is the relaxation of a weakly perturbed circular domain whose initial area fraction is not at equilibrium. This *stable* relaxation to a circle occurs if the applied field h is below the instability value.

Apart from a small correction due to surface tension, the area fraction at long times is $\rho_n\simeq h$ [Fig. 9(d)]. The elementary *elongational* instability of a circular flux domain [Fig. 9(b)] that occurs at higher h is one means by which finite stripes may form in the intermediate state. The area fraction evolves toward $\rho_n=h$, but now the deviation is significant due to larger contributions from the Biot-Savart integral. The curious feature of bulbous tips to the stripe is a rather common observation in dipolar systems. It suggest that the instability is related to the fissioning of the original circle into two smaller ones. Energetic arguments based on this picture show that it rather accurately predicts the onset of this instability.[27] The third phenomenon is the *branching* instability that occurs for still higher values of h [Fig. 9(c)]. The initial condition for this simulation was a circle perturbed with a small-amplitude mode of azimuthal number 3. Rapid growth of that mode is followed by relaxation to ''arms'' of rather uniform width. The angles of the three arms forming the vertex are close to 120°, as is typical in systems governed by surface tension. We conclude from these studies that a physical mechanism to produce the branched and fingered *stationary* shapes of flux domains in the intermediate state is the mechanical instability illustrated in Figs. 9(a)–9(c).

Finally, Fig. 10 shows the effects of surface tension anisotropy on the branching instability of the same initial condition as in Fig. 9(c). While the time evolution first produces

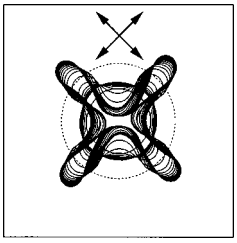

FIG. 10. Branching instability with fourfold surface tension anisotropy ($\epsilon=0.1$). Arrows indicate easy axes.

a fourfold vertex, it subsequently fissions into two threefold vertices that move away from each other. The branches of the pattern have oriented themselves with respect to the low-tension directions determined by the anisotropy (indicated by arrows). The instability of vertices of higher order than three is a common feature of dipolar systems.

V. PERTURBATIONS AROUND THE LAMINAR STATE

In the absence of an in-plane magnetic field, flux domains in the intermediate state often have the shape of buckled laminae. The conformal mapping algorithm for the laminar state is not generalizable to such truly three-dimensional structures and there does not appear to have been any stability calculation of the laminar state. In the following sections we compute the linear stability and linear elastic properties of flux stripes.

A. Energy and stability of a single flux stripe

Consider first a single flux stripe as described by the current-loop model, with width w in the x direction, length l in the y direction, and the plate spacing d. The reduced energy $\widetilde{E}\equiv E/2\sigma_{\rm SN}A$ due to the self- and mutual induction of the currents flowing along the edges is

$$\widetilde{E}=\frac{1}{\alpha}-\frac{N_B}{\alpha}\int_0^\infty d\xi[\Phi(\xi)-\Phi(\sqrt{\xi^2+\alpha^2})], \qquad (5.1)$$

where $\alpha=w/d$ and $N_B=2M^2d/\sigma_{\rm SN}$ is the dimensionless magnetic Bond number. Integration yields

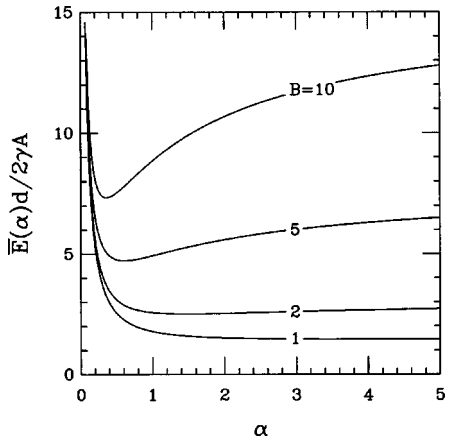

FIG. 11. Stripe energy density as a function of stripe width, for various magnetic Bond numbers.

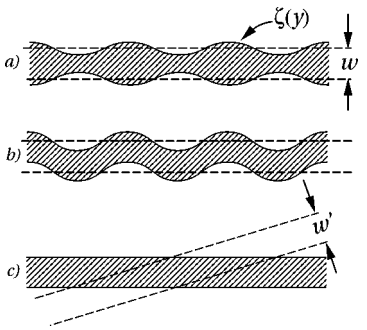

FIG. 12. (a) Peristaltic and (b) serpentine perturbations of a flux stripe. (c) Illustration of the change in stripe width upon a uniform rotation.

$$\widetilde{E}=\frac{1}{\alpha}+\frac{N_B}{4\alpha}[\alpha^2\ \ln(1+\alpha^{-2})+4\alpha\ \tan^{-1}\ \alpha-\ln(1+\alpha^2)]. \tag{5.2}$$

Figure 11 shows $\widetilde{E}(\alpha)$ for various Bond numbers. The minimum of this energy becomes sharper as N_B increases. Minimizing $\widetilde{E}$ with respect to α at fixed area A yields a relation between α and N_B,

$$1-\frac{N_B}{4}[\alpha^2\ \ln(1+\alpha^{-2})+\ln(1+\alpha^2)]=0. \tag{5.3}$$

Now we connect this result to stripe stability. As shown in Figs. 12(a) and 12(b), there are two classes of small distortions. The first (''peristaltic'') involves antisymmetric perturbations and changes the local stripe width. This will be of higher energy than the symmetric (or ''serpentine'') distortions of Fig. 12(b), which preserve the width. It is most convenient to calculate the linearized *force* acting on the interface, using Eq. (4.9).

After a ceremony of relentless algebra we obtain the force associated with a monochromatic perturbation of reduced wave vector $q=dk$; for serpentine perturbations,

$$F_s(q)=q^2-2N_B\left\{\gamma_E+\ln\left(\frac{\alpha q}{2\sqrt{1+\alpha^2}}\right)+K_0(q)+K_0(\alpha q)-K_0(\sqrt{1+\alpha^2}q)\right\}, \tag{5.4}$$

and for the peristaltic perturbation,

$$F_p(q)=q^2-2N_B\left\{-\gamma_E+\ln\left(\frac{\alpha}{\sqrt{1+\alpha^2}}\right)-\ln(q/2)-K_0(q)-K_0(\alpha q)+K_0(\sqrt{1+\alpha^2}q)\right\}. \tag{5.5}$$

In the limit of small q for serpentine perturbations,

$$F_s(q)=\left\{1-\frac{N_B}{4}[\alpha^2\ \ln(1+\alpha^{-2})+\ln(1+\alpha^2)]\right\}q^2-\frac{N_B}{64}\{(1+\alpha^2)^2\ \ln(1+\alpha^2)-\alpha^4\ \ln(\alpha^2)-6\alpha^2\times(1-\tfrac{2}{3}\gamma_E)\}q^4-\frac{N_B}{16}\alpha^2q^4\ \ln(\tfrac{1}{2}q)+O(q^6,q^6\ \ln q). \tag{5.6}$$

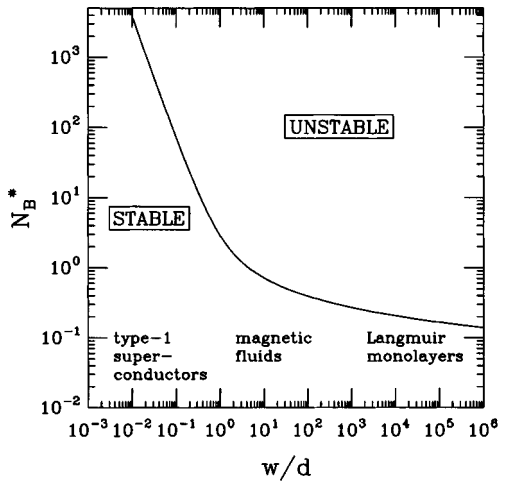

FIG. 13. Critical Bond number for serpentine instability as a function of stripe size. Typical values of w/d are indicated for three experimental systems.

Serendipitously, the condition of stripe equilibrium (5.3) is precisely that which sets the coefficient of q^2 in Eq. (5.6) equal to zero. This can be interpreted as a consequence of rotational invariance. Note that by assigning the same function $\zeta(y)$ to the two edges of the stripe we have maintained its width at w to linear order in ζ, but not to quadratic order (Fig. 12). Now a uniform tilt of the stripe edges $\zeta_y=\text{const}$ [Fig. 12(c)] leads to a width of the rotated stripe $w'=w/\sqrt{1+\zeta_y^2}\simeq w-(w/2)\zeta_y^2+\cdots$. This tilt will cost energy through the ''bulk'' term $E(w)$ in Eq. (5.1) as $E(w')-E(w)\simeq-(w/2)E'(w)\zeta_y^2$, where $E'\equiv dE/dw$. The coefficient of q^2 in Eq. (5.6) is an effective line tension, associated with an energy

$$E=\frac{1}{2}\gamma_{\text{eff}}\int dy\,\zeta_y^2. \tag{5.7}$$

Rotational invariance thus shows that the apparent surface tension vanishes at the equilibrium stripe width. The terms at $O(q^4)$ look like a bending energy,

$$E\sim\frac{1}{2}\int dy\ \zeta_{yy}^2, \tag{5.8}$$

an interpretation spoiled by the term $q^4\ \ln(q)$, which reflects the nonlocality of the magnetic interactions.

The force for peristaltic perturbations has a finite value as $q\to0$ reflecting the compressibility of the stripe. The small-q expansion is

$$F_p=-2N_B\ \ln\left(\frac{\alpha^2}{1+\alpha^2}\right)+\left\{1-\frac{N_B}{2}[\alpha^2\ \ln\alpha-(1+\alpha^2)\times\ln\sqrt{1+\alpha^2}]\right\}q^2+O(q^4,q^4\ \ln q). \tag{5.9}$$

The equilibrium value of the stripe width deduced from Eq. (5.3) defines the boundary of stability of stripes to serpentine perturbations (Fig. 13). At fixed α, instability occurs with increasing N_B and likewise at fixed N_B it sets in with increasing α. The figure shows aspect ratios α corresponding not only to type-I superconductors but also to magnetic fluids (with slab thicknesses and stripe widths in the millimeter to centimeter range) and Langmuir monolayers (with domains tens of micrometer across and a *molecular* thickness).

At its equilibrium width, the energy of small distortions is positive, vanishing as $q \to 0$. It seems impossible to find a field at which the stripe would be unstable to a finite-wavelength mode *if the stripe width has its equilibrium value* (5.3). Fortuitously, the elegant experimental observations on buckling instabilities in Langmuir monolayers[48] have shown what happens when this equilibrium is not reached. Those observations concerned the dynamics of buckling when the temperature was slowly increased. Since these systems are near a critical point of phase separation, small temperature changes produce large changes in the discontinuity in dipole density $\Delta\mu$ between the phases and in the line tension. These directly affect the stability of stripes, quantified by the associated electric Bond number. It was observed that slow temperature ramps produced no buckling, while rapid heating showed buckling. This implicates[49] mass transport as a rate-limiting step as the stripe width adjusts to keep up with the temperature. Under rapid ramps, the width is out of equilibrium, yielding a nonzero (and potentially destabilizing) coefficient of q^2. In the laminar state, we speculate that in the early stages of flux penetration such a mismatch between the actual and equilibrium widths allows the buckling instability to occur.

B. Elastic properties of the laminar state

The CL model can be used to determine the elastic properties of the laminar state by considering as in Fig. 12 small displacements $\zeta_i(y)$ of the SN interfaces. In the long-wavelength (continuum) limit, $\zeta_i(y)$ becomes a displacement field $u(x,y)$, with an elastic free energy

$$\mathcal{F}_{\rm el} = \int d^2r \left[\frac{B}{2} \left(u_x + \frac{1}{2} u_y^2 \right)^2 + \frac{K_1}{2} u_{yy}^2 \right], \qquad (5.10)$$

with B the bulk (compressional) modulus and K_1 the bending modulus. This result applies to serpentine perturbations of the lamina; peristaltic perturbations are gapped like optical phonons and do not contribute to the long-wavelength properties. This form of the free energy could have been anticipated from the single stripe results of Sec. V A; in particular, we see that distortions in the y direction appear as u_{yy}^2 [or $k_y^4 |u(\mathbf{k})|^2$ in Fourier space], again signifying that the effective surface tension is zero. The nonlinear terms are required to preserve the rotational invariance of the free energy (note that we are considering elastic properties in the absence of an in-plane field, although such a field is typically necessary initially to produce the ordered laminae). Equation (5.10) is identical to the elastic free energy of a two-dimensional smectic liquid crystal,[50] a useful analogy as the properties of smectic liquid crystals are well studied; problems such as mechanical instabilities, thermal fluctuation effects, and defect structures have been considered. We expect many of these same phenomena to occur in the laminar state.

Since published calculations exist of the elastic moduli for striped phases in two-dimensional dipolar ferromagnets[51,52] and in ferrofluids[53,54] and the calculation for the laminar phase is identical, we include here only the final results. The bending modulus is

$$K_1 = \frac{3M^2a^3}{8\pi^4} \sum_{m=1}^{\infty} \frac{\sin^2 m\pi h}{m^5} \left\{ 1 - \left[1 + \left(\frac{2\pi dm}{a} \right) + \frac{1}{3} \left(\frac{2\pi dm}{a} \right)^2 \right] e^{-2\pi dm/a} \right\}, \qquad (5.11)$$

where the magnetization is $M = -H_c/4\pi$ and the equilibrium spacing $a = \sqrt{\Delta d / f_{\rm CL}}$, with $f_{\rm CL}(h,d,a)$ given by Eq. (4.8). In the thick-film limit this becomes

$$K_1 = \frac{3M^2a^3}{8\pi^4} \sum_{m=1}^{\infty} \frac{\sin^2 m\pi h}{m^5}. \qquad (5.12)$$

The bulk modulus is

$$B = a^2 \left[\frac{\partial^2 (E_{\rm CL}/A)}{\partial a^2} \right]_h = \frac{4\sigma_{\rm SN} d}{a} - \frac{2M^2 d^2}{a} \ln \left[1 + \frac{\sin^2 \pi h}{\sinh^2(\pi d/a)} \right]. \qquad (5.13)$$

For thick films this becomes $B = 4\sigma_{\rm SN} d/a$. The bending and bulk moduli may be combined to form the length scale $\tilde{\lambda} = \sqrt{K_1/B}$, a persistence length for distortions of the laminar structure (not to be confused with the superconducting penetration depth). In thick films,

$$\tilde{\lambda}^2/a^2 = \frac{3}{32\pi^2} \frac{\sum_{m=1}^{\infty} \sin^2(m\pi h)/m^5}{\sum_{m=1}^{\infty} \sin^2(m\pi h)/m^3}. \qquad (5.14)$$

C. Dislocations in the laminar state

In the laminar state[1] one often observes edge dislocations, where half of a normal lamina has been inserted into the laminar structure. The elastic theory also determines the displacement field of such a dislocation; our calculation closely follows the analogous problem studied in the context of two-dimensional smectic liquid crystals.[55] We begin with the linearized Euler-Lagrange equations for the defect displacement field $u^D(x,y)$,

$$u_{xx}^D - \tilde{\lambda}^2 u_{yyyy}^D = ma\,\delta'(x)\,\theta(y), \qquad (5.15)$$

where the source term on the right-hand side accounts for the presence of the dislocation in such a way that the line integral of ∇u around the dislocation is ma (Burger's vector), with m the number of half sheets inserted and a the lamina

spacing. Solving Eq. (5.15) with Fourier transforms,[55] the result is $u^D(x,y)=mG(\mathbf{r})$, with

$$G(\mathbf{r})=\frac{a}{4}\,\mathrm{sgn}(x)[\mathrm{erf}(y/\sqrt{4\tilde{\lambda}|x|})+1]. \tag{5.16}$$

For a collection of dislocations centered at $\{\mathbf{r}_i\}$ with strengths $\{m_i\}$, we may introduce the dislocation density $m(\mathbf{r})=\Sigma_i m_i\delta(\mathbf{r}-\mathbf{r}_i)$, so that the displacement field is obtained by linear superposition, $u^D(\mathbf{r})=\int d^2r' m(\mathbf{r}')G(\mathbf{r}-\mathbf{r}')$. The free energy $\mathcal{F}_D$ of the defects is then obtained by substituting u^D into the the elastic free energy and using the ''harmonic conjugate'' trick of Toner and Nelson.[55] The final result is

$$\mathcal{F}_D=\frac{1}{2}\int d^2r_1\int_{|\mathbf{r}_1-\mathbf{r}_2|>a} d^2r_2 m(\mathbf{r}_1)m(\mathbf{r}_2)U(\mathbf{r}_1-\mathbf{r}_2) + E_D\int d^2r m^2(\mathbf{r}), \tag{5.17}$$

where the interaction potential is

$$U(\mathbf{r})=\frac{a^2B}{4}\left(\frac{\tilde{\lambda}}{\pi|x|}\right)^{1/2}e^{-y^2/4\tilde{\lambda}|x|} \tag{5.18}$$

and the defect core energy is

$$E_D=\frac{B}{2}\int d^2r[\tilde{\lambda}^2(G_{yy})^2+(G_x)^2]=\frac{1}{8\sqrt{\pi}}Ba^2\left(\frac{\tilde{\lambda}}{a}\right)^{1/2}. \tag{5.19}$$

The core energy can be calculated as a function of the reduced field h by using the results of Sec. V B [Eqs. (5.13) and (5.14)]. A rough estimate shows that this energy is generally of order $10^{-3}(H_c^2/8\pi)a^3$ and can therefore be quite small; as a result, it should be easy to nucleate dislocations in the laminar phase.

VI. DISCUSSION

The free-boundary approach to the intermediate state has led to a picture of the shape instabilities of individual flux domains and ordered arrays. In addition, the correspondence with smectic liquid crystals suggests phenomena that should occur in type-I superconductors. Below we suggest experiments to visualize these effects, starting from the ordered laminar state. Experiments by Reisin and Lipson[56] have shown some of these.

(i) The buckling instability. Rapid changes in the applied normal field may allow buckling instabilities to occur in much the same way as observed in Langmuir monolayers. Of interest would be the dependence of buckling wavelength on the magnitude of the field jump.

(ii) The chevron instability. If the in-plane magnetic field is applied at an angle with respect to the laminae, we expect an instability toward a zigzag or chevron pattern as the laminae attempt to reorient. This is like the Helfrich-Hurault effect in smectic liquid crystals,[50] wherein a field component normal to smectic layers, producing a torque on them, induces an undulatory instability.

(iii) The Eckhaus instability. If the normal magnetic field is slowly changed in magnitude the stripe width and spacing must adjust to stay in equilibrium. As in convective systems,[57] this may occur through an Eckhaus-like nucleation phenomenon to create or destroy laminae. Dislocations can be produced that will move toward the sample edges or annihilate at the center in accord with the direction in which the wavelength must adjust. Their climb and glide dynamics will provide an important testing ground for the theory of interface dynamics.

(iv) Critical-point effects. In the simplified contour dynamics in which the local field is taken to be H_c, the Bond number depends only on the ratio $d/\Delta(T)$. Near the zero-field superconductor-normal critical temperature the interfacial width $\Delta(T)$ diverges as $(T_c-T)/T_c$. This should produce characteristic changes in the equilibrium stripe width as well as possible instabilities.

We close by emphasizing what has *not* been accomplished here. First, we have considered laterally infinite samples, ignoring the whole issue of flux penetration at the edges. This can be very significant in both type-I and type-II superconductors.[58] A treatment of these effects requires not only the electromagnetics of fields near the slab edges but also consideration of processes such as domain fission. Second, we have presented an oversimplified dynamical picture in which diffusional instabilities are absent. The interplay between the Mullins-Sekerka and these mechanical instabilities has not been considered theoretically and may shed light on various problems in flux domain pattern formation. Third, a large-scale numerical study of the many-domain problem has not been attempted, precluding a clear understanding of the true ''energy landscape'' of this strongly interacting system. Fourth, the effects of in-plane components to the applied magnetic fields have not been incorporated into the free-boundary approach in any quantitative way. This will be important for an understanding of the instabilities described above. Fifth, the extension of matched asymptotic methods used in purely two-dimensional systems to the slab geometry of the intermediate state has not been developed and would greatly clarify the free-boundary approach to flux domain shapes. Finally, coarse-graining approaches to domain dynamics analogous to Otto and Kohn's recent study of magnetic fluid pattern formation[59,60] may prove quite fruitful.

ACKNOWLEDGMENTS

We are grateful to C.-Y. Mou, Thomas R. Powers, and John Toner for important discussions on the energetics of the intermediate state, to O. Narayan and H. Bokil for communication of Ref. 18 prior to publication, and to C. Reisin and S. G. Lipson for sharing with us the results of their ongoing experiments. This work was supported in part by NSF PFF Grants Nos. DMR 93-50227 (R.E.G.), DMR 92-23586 (A.T.D.) and 96-28926 (A.T.D) and the Alfred P. Sloan Foundation (R.E.G. and A.T.D.).

*Electronic mail: dorsey@phys.ufl.edu
†Electronic mail: gold@physics.arizona.edu.

[1] R. P. Huebener, *Magnetic Flux Structures in Superconductors* (Springer-Verlag, New York, 1979).
[2] T. E. Faber, Proc. R. Soc. London, Ser. A **248**, 460 (1958).
[3] F. Haenssler and L. Rinderer, Helv. Phys. Acta **40**, 659 (1967).
[4] R. N. Goren and M. Tinkham, J. Low Temp. Phys. **5**, 465 (1971).
[5] R. P. Huebener, R. T. Kampwirth, and V. A. Rowe, Cryogenics **12**, 100 (1972).
[6] I. V. Sharvin, Sov. Phys. JETP **6**, 1031 (1958).
[7] L. D. Landau, Sov. Phys. JETP **7**, 371 (1937).
[8] E. R. Andrew, Proc. R. Soc. London, Ser. A **194**, 98 (1948); K. Maki, Ann. Phys. (N.Y.) **34**, 363 (1965); G. Lasher, Phys. Rev. **154**, 345 (1967); D. J. E. Callaway, Ann. Phys. (N.Y.) **213**, 166 (1992).
[9] H. Frahm, S. Ullah, and A. T. Dorsey, Phys. Rev. Lett. **66**, 3067 (1991).
[10] F. Liu, M. Mondello, and N. Goldenfeld, Phys. Rev. Lett. **66**, 3071 (1991).
[11] A. B. Pippard, Philos. Mag. **41**, 243 (1950).
[12] W. W. Mullins and R. F. Sekerka, J. Appl. Phys. **35**, 444 (1964).
[13] A. T. Dorsey, Ann. Phys. (N.Y.) **233**, 248 (1994); J. C. Osborn and A. T. Dorsey, Phys. Rev. B **50**, 15 961 (1994); S. J. Chapman, Q. Appl. Math. **53**, 601 (1995).
[14] J. Pearl, Appl. Phys. Lett. **5**, 65 (1964).
[15] A. L. Fetter and P. C. Hohenberg, Phys. Rev. **159**, 330 (1967).
[16] R. E. Goldstein, D. P. Jackson, and A. T. Dorsey, Phys. Rev. Lett. **76**, 3818 (1996).
[17] For a review, see D. A. Kessler, J. Koplik, and H. Levine, Adv. Phys. **37**, 255 (1988).
[18] See H. Bokil and O. Narayan, Phys. Rev. B **56**, 11 195 (1997).
[19] M. Seul and D. Andelman, Science **267**, 476 (1995).
[20] R. E. Rosensweig, M. Zahn, and R. Shumovich, J. Magn. Magn. Mater. **39**, 127 (1983).
[21] A. O. Tsebers and M. M. Mairov, Magnetohydrodynamics **16**, 21 (1980).
[22] A. J. Dickstein, S. Erramilli, R. E. Goldstein, D. P. Jackson, and S. A. Langer, Science **261**, 1012 (1993).
[23] S. A. Langer, R. E. Goldstein, and D. P. Jackson, Phys. Rev. A **46**, 4894 (1992).
[24] D. P. Jackson, R. E. Goldstein, and A. O. Cebers, Phys. Rev. E **50**, 298 (1994).
[25] D. Andelman, F. Brochard, and J.-F. Joanny, J. Chem. Phys. **86**, 3673 (1987).
[26] K. Y. C. Lee and H. M. McConnell, J. Phys. Chem. **97**, 9532 (1993).
[27] R. E. Goldstein and D. P. Jackson, J. Phys. Chem. **98**, 9626 (1994).
[28] M. Seul, L. R. Monar, L. O'Gorman, and R. Wolfe, Science **254**, 1616 (1991).
[29] D. M. Petrich and R. E. Goldstein, Phys. Rev. Lett. **72**, 1120 (1994).
[30] R. E. Goldstein, D. J. Muraki, and D. M. Petrich, Phys. Rev. E **53**, 3933 (1996).
[31] A. Hagberg and E. Meron, Phys. Rev. Lett. **72**, 2494 (1994).
[32] C. B. Muratov and V. V. Osipov, Phys. Rev. E **53**, 3101 (1996).
[33] K. J. Lee, W. D. McCormick, Q. Ouyang, and H. L. Swinney, Science **261**, 192 (1993).
[34] K. J. Lee and H. L. Swinney, Phys. Rev. E **51**, 1899 (1995).
[35] R. FitzHugh, Biophys. J. **1**, 445 (1961); J. S. Nagumo, S. Arimoto, and Y. Yoshizawa, Proc. IRE **50**, 2061 (1962); R. FitzHugh, in *Biological Engineering*, edited by H. P. Schwan (McGraw-Hill, New York, 1969).
[36] L. M. Milne-Thomson, *Theoretical Hydrodynamics*, 5th ed. (MacMillan Press Ltd., London 1968), Chaps. XI and XII.
[37] G. Birkhoff and E. H. Zarantonello, *Jets, Wakes, and Cavities* (Academic Press, New York, 1957).
[38] L. D. Landau, E. M. Lifshitz, and L. P. Pitaevskii, *Electrodynamics of Continuous Media*, 2nd ed. (Pergamon Press, New York, 1984), p. 119.
[39] A. Fortini and E. Paumier, Phys. Rev. B **5**, 1850 (1972).
[40] The energy of a sample of volume V with a uniform magnetization $\mathbf{M}$ in an external field $\mathbf{H}_a$ is $-\frac{1}{2}\mathbf{M}\cdot\mathbf{H}_a V$. For a superconductor, $\mathbf{M}=-\mathbf{H}_n/4\pi$, so that the energy per unit area of the sample is $H_n H_a d/4\pi$.
[41] This ignores the added area of the SN interface due to the flaring of the normal domains.
[42] C.-Y. Mou (private communication).
[43] C. Kooy and V. Enz, Philips Res. Rep. **15**, 7 (1960).
[44] J. A. Cape and G. W. Lehman, J. Appl. Phys. **42**, 5732 (1971).
[45] See A. A. Abrikosov, *Fundamentals of the Theory of Metals* (North-Holland, Amsterdam, 1988), p. 479.
[46] For a discussion of surface tension anisotropy within the context of dendritic growth see Ref. 17.
[47] A. Bodmer, U. Essman, and H. Träuble, Phys. Status Solidi A **13**, 471 (1972); A. Bodmer, *ibid.* **19**, 513 (1973).
[48] K. J. Stine, C. M. Knobler, and R. C. Desai, Phys. Rev. Lett. **65**, 1004 (1990).
[49] A. O. Cebers and R. E. Goldstein (unpublished).
[50] W. Helfrich, Appl. Phys. Lett. **17**, 531 (1970); J. P. Hurault, J. Chem. Phys. **59**, 2086 (1973); see also P. G. de Gennes and J. Prost, *The Physics of Liquid Crystals* (Oxford University Press, New York, 1993), pp. 361–364.
[51] A. Kashuba and V. L. Pokrovsky, Phys. Rev. Lett. **70**, 3155 (1993); Phys. Rev. B **48**, 10 335 (1993). Some errors in the calculation of the bending modulus are corrected in Appendix A of Ar. Abanov, V. Kalatsky, V. L. Pokrovsky, and W. M. Saslow, Phys. Rev. B **51**, 1023 (1995).
[52] K.-O. Ng and D. Vanderbilt, Phys. Rev. B **52**, 2177 (1995).
[53] A. Cebers, J. Magn. Magn. Mater. **149**, 93 (1995).
[54] C. Flament, J. C. Bacri, A. Cebers, F. Elias, and R. Perzynski, Europhys. Lett. **34**, 225 (1996).
[55] J. Toner and D. R. Nelson, Phys. Rev. B **23**, 316 (1981).
[56] C. R. Reisin and S. G. Lipson (unpublished), and private communication.
[57] M. C. Cross and P. C. Hohenberg, Rev. Mod. Phys. **65**, 851 (1993).
[58] C. A. Duran, P. L. Gammel, R. E. Miller, and D. J. Bishop, Phys. Rev. B **52**, 75 (1995).
[59] F. Otto, Arch. Ration. Mech. Anal. (to be published).
[60] R. V. Kohn and F. Otto, Physica D **107**, 272 (1997).